MAGNETOHYDRODYNAMICS Vol. 57 (2021), No. 4, pp. 423–435
DOI: 10.22364/mhd.57.4.1

EFFECT OF THE HARTMANN NUMBER ON MHD STOKES FLOW IN A LID-DRIVEN CAVITY

Ebutalib Çelik

Çanakkale Onsekiz Mart University, Department of Computer Technologies, Çanakkale, Turkey

A two-dimensional steady, incompressible and electrically conducting Stokes flow in a lid-driven rectangularly confined region is considered. A boundary value problem is formulated for a cavity with the upper lid moving with a constant velocity ($u = 1$) and the lower lid moving with an S velocity. The finite difference method is applied to generate solutions for the governing equations of the flow in the region. Moreover, streamline bifurcation under a magnetic field of different strengths applied in the x- or y-direction and the effect of the Hartmann number on the eddy formation are investigated.

Introduction.

Magnetohydrodynamics (MHD) is a popular research field in fluid mechanics that has several important applications in engineering and industry. Some of these include MHD accelerators and generators, space propulsion, electromagnetic pumps, cooling systems with liquid metals, etc. MHD examines the motion of electrically conducting fluids under a magnetic field in a cavity with a moving lid. Along with the slipping wall, the magnetic field directs the flow and can control the flow motion.

Many numerical methods have been developed to solve the governing equations of MHD flow in different configurations of interest. Some of them are the boundary element method (BEM) [1–4], the finite element method (FEM) [5–8] and the method of radial basis function collocation [9, 10]. Additionally, the finite difference method (FDM) that gives influential results in the solution of the boundary value problem is also applied. Sterl [11] used the finite difference code to analyzed the behavior of MHD flows at high Hartmann numbers in a two-dimensional (2D) square duct by investigating the influence of the Hartmann number M, wall conductance ratio c and varying magnetic field. Hsieh *et al.* [12] proposed an improvement of the finite difference method, called the tailored finite point method, and solved the steady MHD duct flow problems with a high Hartmann number. Using the finite difference method, Chutia and Deka [13] investigated a steady two-dimensional (2D) MHD flow through a square duct under the action of a transverse magnetic field acting with an inclination to the duct walls. Arslan and Tezer-Sezgin [14] considered an MHD flow in a long channel along the z-axis under an external magnetic field which was perpendicular to the channel axis and demonstrated the effects of the Hartmann number, conductivity parameter and slip length on the behavior of both the velocity and the induced magnetic field using FDM.

The coupling of the continuity equation, the Navier–Stokes equations of hydrodynamics and the Maxwell electromagnetic equations governs the MHD flow. In this study, some physical assumptions have been made, such as the high viscous flow ($\mathrm{Re} \ll 1$) and the negligible magnetic field ($\mathrm{Rm} \ll 1$) in the fluid. This is a Stokes approximation and it is going to be called as MHD Stokes. Gürbüz and Tezer-Sezgin [15] solved the MHD Stokes flow equations in a lid-driven cavity and in a backward-facing step channel exposed to a uniform magnetic field. In the cavity, they found that with the increase of the Hartmann number, the boundary layers were formed closer to the moving lid and

secondary recirculation appears in the rest of the cavity. Okechi *et al.* [16] considered an MHD flow through a wavy-curved channel filled with an electrically conducting fluid and investigated the effects of the wavy boundaries, channel radius of curvature and applied magnetic field on the flow. Okechi and Asghar [17] also modelled a flow through a corrugated curved channel and assumed that the flow was perpendicular to the corrugations in the presence of a magnetic field. Gürbüz and Tezer-Sezgin [10] obtained numerical results for a constricted enclosure under the effect of a magnetic field with several values of the Hartmann number and constriction ratio.

Cavity type flow problems are used to analyze the flow behavior as well as a benchmark of the developed numerical methods. Shankar [18] considered the Stokes flow in a rectangular 2D cavity in which the flow was driven by the upper lid. He focused on the eddy pattern in the cavity and examined the relationship of the corner eddies with the main eddy using an analytical method. Kelmanson and Lonsdale [19] presented an integral-equation method and applied it to the lid-driven-cavity eddies, two of which were moving opposite to each other with a distinct velocity. They observed a variety of topologically distinct flow patterns with variations in the wall velocity. Gürcan *et al.* [20] investigated the Stokes flow in a rectangular driven cavity of depth $2H$ and width $2L$, where the two lids moved in opposite directions with velocities U_1 and U_2, respectively. They set-forth a new class of flow patterns with respect to the variation of the aspect ratio $\mathrm{A} = H/L$ and velocity ratio $\mathrm{S} = U_1/U_2$ and constructed a control space diagram (S, A) to reveal the interaction of these patterns. Gürcan [21] also found the effect of the Reynolds number (Re) on the streamline patterns and their bifurcations in a double-lid-driven cavity with free surfaces. Streamline topology and eddy genesis in cavities with different geometric shapes can be found in [22–25].

In this paper, we analyze the flow bifurcation of the MHD Stokes flow in a rectangular cavity exposed to a uniform magnetic field. The flow motion can be controlled with the help of two parameters, such as the height of the region h and the strength of the magnetic field M. The motivation behind this study is that the behavior of the Stokes flow in the presence of a uniform magnetic field has not been qualitatively investigated yet. We work on coupled governing equations and compute them iteratively using the FDM, which is a classical approach and has proven to be very efficient in terms of both programming and low computational costs. The main goal of this work is to introduce a mechanism for flow transformations in the flow domain as h varies with different Hartmann numbers M.

1. Problem formulation and boundary values.

It is assumed that the electrically conducting fluid in a rectangular cavity is steady, incompressible and viscous. The flow interacts with the external applied magnetic field imposed horizontally or vertically. h is the parameter of the height of the region, whose width is constant starting from the origin. The cavity has two stationary side walls, two moving lids, namely, the upper lid that has a constant velocity $u = 1$ and the lower lid moving with the velocity $u = \mathrm{S}$. Here, three different cases of S will be examined, i.e. $\mathrm{S} = -1, 0, 1$. The setup of the 2D flow problem is shown in Fig. 1.

The non-dimensional MHD equations are given as

$$\nabla \cdot \mathbf{u} = 0, \tag{1}$$

$$\mathrm{Re}\,(\mathbf{u} \cdot \nabla)\,\mathbf{u} = -\nabla p + \nabla^2 \mathbf{u} + \mathrm{M}^2\,(-\nabla\phi + \mathbf{u} \times \mathbf{H}) \times \mathbf{H}, \tag{2}$$

$$\mathrm{Rm}\,(-\nabla\phi + \mathbf{u} \times \mathbf{H}) = \nabla \times \mathbf{H}, \tag{3}$$

where $\mathbf{u} = (u, v, 0)$, $\mathbf{H} = (H_x, H_y, H_z)$, p, $\mathbf{J}$ and ϕ are, respectively, the fluid velocity, the

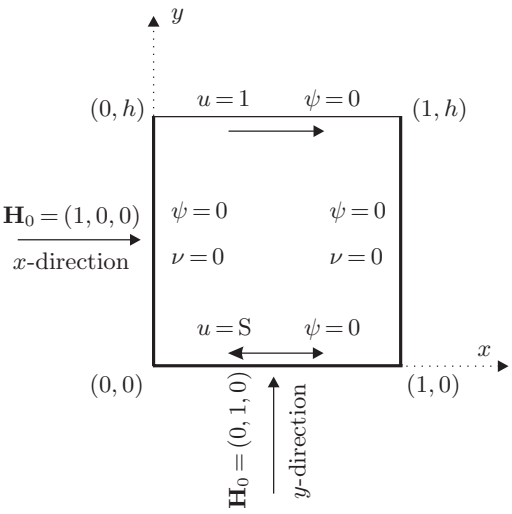

Fig. 1. Schematic of the flow problem and boundary values.

magnetic field, the fluid pressure, the electric current density and the electric potential. Since we assume the negligibility of the induced magnetic field (Rm $\ll$ 1), Eq. (3) will no longer be used for the solution procedure. The Stokes approximation requires small values of the Reynolds number, so the MHD Stokes flow equations can be derived by omitting the convective terms in Eq. (2) as follows,

$$\nabla \cdot \mathbf{u} = 0, \tag{4}$$

$$0 = -\nabla p + \nabla^2 \mathbf{u} + \mathrm{M}^2 \left(-\nabla\phi + \mathbf{u} \times \mathbf{H}\right) \times \mathbf{H}. \tag{5}$$

Since it is assumed that the magnetic field is applied horizontally or vertically, the Laplace equation for the electric potential ($\nabla^2\phi = 0$) is derived from the Ohm's law and conservation of the electric current $\nabla \cdot \boldsymbol{J} = 0$. With uniform boundary conditions, the solution becomes the zero electric potential, $\phi = 0$, by omitting the gradient of the electric potential in Eq. (5), $\nabla\phi = 0$.

For the magnetic field imposed on the flow region in the x-direction, $\mathbf{H}_0 = (1, 0, 0)$, the governing Eqs. (4)–(5) are modified as

$$\frac{\partial u}{\partial x} + \frac{\partial v}{\partial y} = 0, \tag{6}$$

$$\nabla^2 u = \frac{\partial p}{\partial x}, \tag{7}$$

$$\nabla^2 v = \frac{\partial p}{\partial y} + \mathrm{M}^2 v. \tag{8}$$

In the 2D incompressible flow, a stream function/vorticity formulation can be derived by introducing the stream function ψ and the vorticity ω from the following relations

$$u = \frac{\partial \psi}{\partial y}, \qquad v = -\frac{\partial \psi}{\partial x}, \qquad \omega = \frac{\partial v}{\partial x} - \frac{\partial u}{\partial y}. \tag{9}$$

It is clear that we derive the Poisson equation for the stream function as $\nabla^2\psi = -\omega$. By cross-differentiating Eqs. (7) and (8), the vorticity Poisson equation is derived as $\nabla^2\omega = \mathrm{M}^2\partial v/\partial x$. Thus, the governing equations for the MHD Stokes flow are given for the primitive variables ψ, ω as

$$\begin{aligned} \nabla^2\psi &= -\omega, \\ \nabla^2\omega &= \mathrm{M}^2\frac{\partial v}{\partial x}. \end{aligned} \tag{10}$$

Similarly, since $\mathbf{H}_0 = (0, 1, 0)$ for the magnetic field in the y-irection, Eq. (5) takes the form

$$\nabla^2 v = \frac{\partial p}{\partial y}, \qquad \nabla^2 u = \frac{\partial p}{\partial x} + \mathrm{M}^2 u, \tag{11}$$

which yields the following Poisson-type system of equations

$$\begin{aligned} \nabla^2\psi &= -\omega, \\ \nabla^2\omega &= -\mathrm{M}^2\frac{\partial u}{\partial y}. \end{aligned} \tag{12}$$

From the no-slip conditions of the stationary and sliding wall, the corresponding boundary conditions of Eqs. (10)–(12) are written in terms of the velocity and stream function as follows:
(a) $\psi = \mathrm{const} = 0$ at all boundaries:

$$\psi(0, y) \;=\; \psi(1, y) \;=\; \psi(x, 0) \;=\; \psi(x, h) \;=\; 0 \tag{13}$$

(b) No-slip on the upper and lower lids:

$$u = \frac{\partial\psi}{\partial y}(x, h) = 1, \qquad u = \frac{\partial\psi}{\partial y}(x, 0) = S, \tag{14}$$

(c) and on the side walls:

$$v = \frac{\partial\psi}{\partial x}(0, y) = \frac{\partial\psi}{\partial x}(1, y) = 0. \tag{15}$$

Since the boundary conditions are known in terms of velocity components, the boundary values of the only non-vanishing vorticity component can be derived in terms of the stream function. It is known that $\nabla^2\psi = -\omega$, so

$$\omega = -\frac{\partial^2\psi}{\partial x^2} - \frac{\partial^2\psi}{\partial y^2} \equiv -\frac{\partial u}{\partial y} + \frac{\partial v}{\partial x}. \tag{16}$$

No-penetration boundary conditions require that the component of the velocity normal to the walls is zero. Enforcing the boundary conditions for the velocity, for example, $v = 0$ and thus $\partial v/\partial x = 0$ over the top and bottom yields

$$\omega = -\frac{\partial u}{\partial y} = -\frac{\partial\psi^2}{\partial y^2}. \tag{17}$$

In a similar fashion, the relation for the boundary value at the side walls is derived as

$$\omega = \frac{\partial v}{\partial x} = -\frac{\partial\psi^2}{\partial x^2}. \tag{18}$$

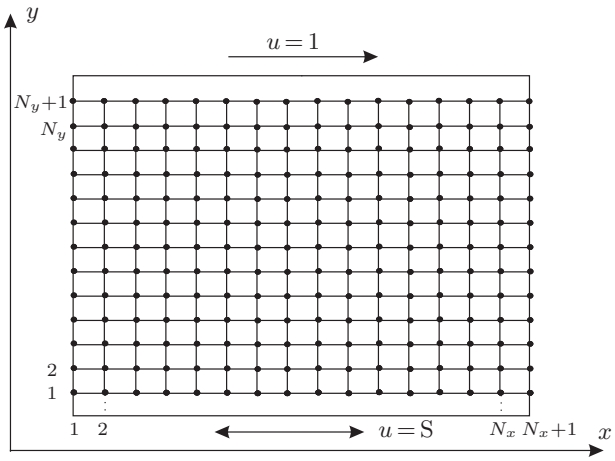

Fig. 2. A finite difference grid used to calculate the lid-driven cavity flow under a magnetic field.

2. Numerical solution.

The governing equations (10)–(12) given in Chapter 1 have no analytical solution unless it is known. Therefore, the finite difference method was used to solve these equations with the corresponding boundary conditions (13)–(15). In this section, a finite difference formulation of the system (10) is presented, and similar operations can be performed for those in Eq. (12).

The flow domain is gridded uniformly, as shown in Fig. 2. The central difference of second-order partial derivatives with respect to x and y is used to approximate the solution:

$$\left(\frac{\partial^2\phi}{\partial x^2}\right)_{i,j} \simeq \frac{\phi_{i-1,j} - 2\phi_{i,j} + \phi_{i+1,j}}{\Delta x^2}, \qquad \left(\frac{\partial^2\phi}{\partial y^2}\right)_{i,j} \simeq \frac{\phi_{i,j-1} - 2\phi_{i,j} + \phi_{i,j+1}}{\Delta y^2}. \tag{19}$$

The discrete form of Eqs. (10) for the stream function and vorticity is

$$\psi_{i+1,j} - 2(1+\beta)\psi_{i,j} + \psi_{i-1,j} + \beta\psi_{i,j+1} + \beta\psi_{i,j-1} + \Delta x^2\omega_{i,j} = 0, \tag{20}$$

$$\omega_{i+1,j} - 2(1+\beta)\omega_{i,j} + \omega_{i-1,j} + \beta\omega_{i,j+1} + \beta\omega_{i,j-1} + \Delta x^2 N_{i,j} = 0, \tag{21}$$

using the approximation (19), where $\beta = (\Delta x/\Delta y)^2$ and $N_{i,j}$ is the non-uniform term of the vorticity equation in Eqs. (10).

The Taylor series expansion of the stream function is used to evaluate the boundary values of the vorticity. So, for example, considering the expansion at the grid node just below the top lid yields

$$\psi_{i,N_y} \simeq \psi_{i,N_{y+1}} - \Delta y\left(\frac{\partial\psi}{\partial y}\right)_{i,N_y+1} + \frac{1}{2}\Delta y^2\left(\frac{\partial^2\psi}{\partial y^2}\right)_{i,N_y+1}. \tag{22}$$

It is known that

$$\left(\frac{\partial\psi}{\partial y}\right)_{i,N_y+1} = 1 \quad \text{and} \quad \omega_{i,N_y+1} = -\left(\frac{\partial^2\psi}{\partial y^2}\right)_{i,N_y+1},$$

then, solving for ω_{i,N_y+1} yields

$$\omega_{i,N_y+1} = 2\frac{\psi_{i,N_{y+1}} - \psi_{i,N_y}}{\Delta y^2} - 2\frac{1}{\Delta y}.$$

We can evaluate the values of the vorticity by a similar approach using

$$\omega_{1,j} = 2\frac{\psi_{1,j} - \psi_{2,j}}{\Delta x^2}, \qquad \omega_{N_x+1,j} = 2\frac{\psi_{N_x+1,j} - \psi_{N_x,j}}{\Delta x^2} \tag{23}$$

at the side wall, and

$$\omega_{i,1} = 2\frac{\psi_{i,1} - \psi_{i,2}}{\Delta y^2} - 2\frac{S}{\Delta y}$$

at the bottom lid. In the implementation, the coupled MHD Stokes equations (10) with a subject boundary condition are solved iteratively by using their discretized form in Eqs. (20)–(21). To obtain a more accurate solution, a third-order Taylor series expansion was applied to Eq. (22). Also, to improve the rate of convergence, e.g., for the stream function, $\psi_{i,j}^{l+1} = \psi_{i,j}^{l} + \delta[2(1+\beta)]^{-1}R_{i,j}^{l}$ is used, where the relaxation factor $\delta = 0.5$ and $R_{i,j}^{l}$ is the value of the residual at the k-th iteration. The computational process is continued until a difference between the consecutive values of the solution is obtained within the preassigned tolerance $\varepsilon = 10^{-9}$. Numerical solutions were performed using the Matlab programming [26].

3. Results and discussions.

The effect of the magnetic field applied to a rectangular region from both the y-direction and the x-direction on the streamline is investigated. When Eqs. (10) and (12) are examined, it is seen that the flow is Stokes-like if the Hartmann number is $M = 0$. Two parameters controlling the flow in the region are the depth of the cavity and the Hartmann number. The flow bifurcates at the degenerate critical point with varying parameters, namely, the type or the number of stationary point changes. We use the term flow bifurcation to describe such changes in configuration.

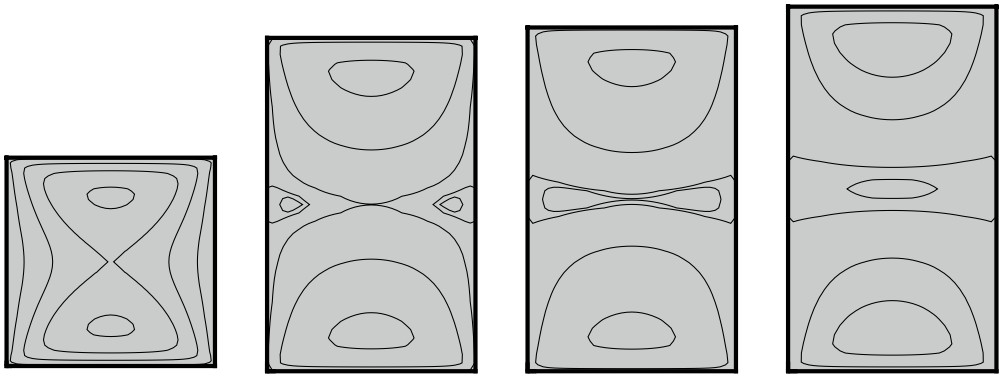

Fig. 3. Streamline patterns for $M = 10$ and $S = -1$ obtained by FDM in a 40×40 grid: (*a*) $h = 1.0$, (*b*) $h = 1.6$, (*c*) $h = 1.65$, (*d*) $h = 1.75$.

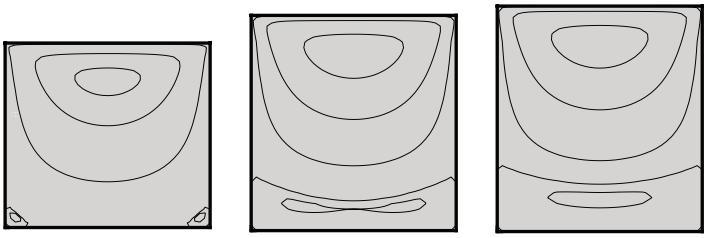

(*a*) (*b*) (*c*)

Fig. 4. Streamline patterns for M = 10 and S = 0 obtained by FDM in a 40×40 grid: (*a*) $h = 0.95$, (*b*) $h = 1.05$, (*c*) $h = 1.1$.

Table 1. Comparison of h values at which the flow pattern changes in the cavity at S = –1.

M = 0 (FDM)	M = 0 ([20])	M = 10
$h_{\mathrm{B.M}} = 2.53$	$h_{\mathrm{B.M}} = 2.498$	$h_{\mathrm{B.M}} = 1.52$
$h_{\mathrm{G.B}} = 2.81$	$h_{\mathrm{G.B}} = 2.789$	$h_{\mathrm{G.B}} = 1.64$
$h_{\mathrm{C.B}} = 2.93$	$h_{\mathrm{C.B}} = 2.91$	$h_{\mathrm{C.B}} = 1.70$

3.1. Results on the magnetic field acting in the x-direction. In this section, the effect of the magnetic field acting in the x-direction on the streamlines and new eddy formation in the region was examined at $\mathrm{S} = -1, 0.1$. Fig. 3 illustrates a sequence of flow patterns for M = 10 and S = −1 (i.e. the lids moving with an equal velocity but in opposite directions).

As shown in Fig. 3, there is a separatrix with a saddle at the center of the region and two centers symmetrical with respect to the point (0.5, 0.5) for M = 10 and $h = 1$. Two degenerate critical points appear on the two side walls at a critical value of $h_{\mathrm{B.M}} = 1.52$ and then separation bubbles emerge on them. As the height of the cavity gradually increases, the side eddies grow up together and approach the saddle point at the center of the field. A global bifurcation arises at $h_{\mathrm{G.B}} = 1.64$ which involves the formation of two saddle-point triangles as a result of the different saddle-saddle connections. At the critical value $h_{\mathrm{C.B}} = 1.7$, the number of eddies increases to three when the separatrix between the lower and upper center turns into the complete eddy.

It is seen that this bifurcation sequence obtained for M = 10 is the same for M = 0. The h values at which bifurcation occurs for M = 0 and M = 10 are summarized in Table 1. When comparing these values, it can be easily seen that the Hartmann number causes a decrease in the height values. While the flow topology does not change until $h = 2.5$ for M = 0, the new eddy formation is completed at $h = 1.7$ for M = 10.

A rectangular domain with the upper lid-driven S = 0 and M = 10 was considered. A series of bifurcations that occur at the stagnation points with the enlargement of the cavity's length is shown in Fig. 4. There is a single eddy with its center-line and two corner eddies in the flow. As h increases, the corner eddies grow in size and at $h = 1$ these two eddies undergo a saddle-point bifurcation at the midpoint of the lower wall. Thus, the critical points on the wall pass into the flow and the number of stationary points of the region increases. As h increases, the saddle point shifts towards the center of the cavity, while the lower eddies continue to get closer, forming the second complete eddy within the cavity at $h = 1.7$. This transformation in streamlines was observed in cavites of different shapes and was the same as for M = 0. The h values at which the structural

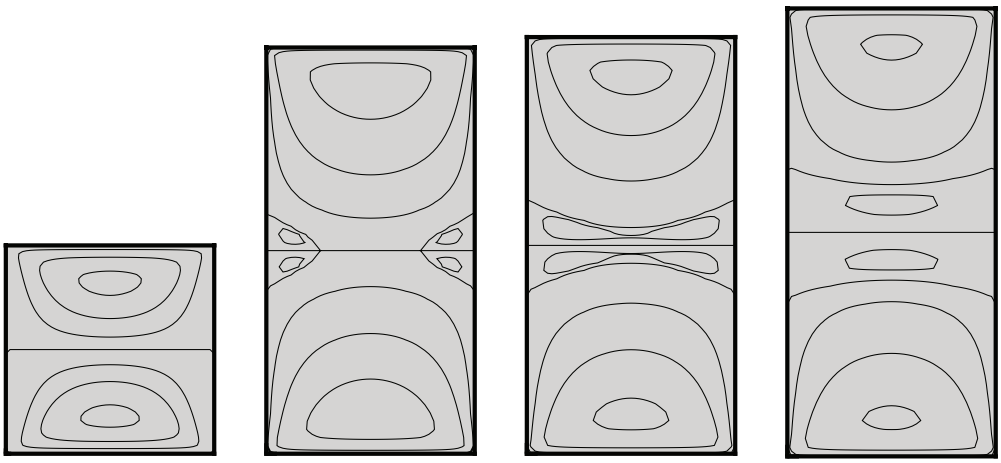

Fig. 5. Streamline patterns for M = 10 and S = 1 obtained by FDM in a 50 × 50 grid: (*a*) $h = 1.0$, (*b*) $h = 1.95$, (*c*) $h = 2.0$, (*d*) $h = 2.15$.

Table 2. Comparison of h values at which the flow pattern changes in the cavity at S = 0.

	M = 0 (FDM)	M = 0	M = 10
Second vortex		[18]	
	$h_{\mathrm{S.N}} = 1.65$	$h_{\mathrm{S.N}} = 1.62975$	$h_{\mathrm{S.N}} = 1.0$
	$h_{\mathrm{C.B}} = 1.8$	$h_{\mathrm{C.B}} = 1.8$	$h_{\mathrm{C.B}} = 1.08$
Third vortex		[27]	
	$h_{\mathrm{S.N}} = 3.06$	$h_{\mathrm{S.N}} = 3.028$	$h_{\mathrm{S.N}} = 1.83$
	$h_{\mathrm{C.B}} = 3.23$	$h_{\mathrm{C.B}} = 3.202$	$h_{\mathrm{C.B}} = 1.91$

transformations occurred at stagnation points for the second or even for the third vortex are listed in Table 2 for M = 0 and M = 10.

As h increases with S = 1, at which the lids move in the same direction, there arise three different bifurcations in the critical value $h_{B.\mathrm{M}}$, $h_{\mathrm{G.B}}$, $h_{\mathrm{C.B}}$. From $h = 1$ to $h = 1.87$, the flow contains a separation line ($\psi = 0$) that divides the flow field in halves with two symmetrical main eddies. At $h_{B\mathrm{M}} = 1.87$, symmetrically located separation bubbles appear on the side walls of the cavity. These bubbles approach each other as h increases gradually and coalesce in the middle of the field at $h_{\mathrm{G.B}} = 1.99$ to produce a separatrix with a saddle point and two centers. These center points get closer to become a center simultaneously with the saddle point at $h_{\mathrm{C.B}} = 2.07$. There are now four fully developed vortices in the cavity. As seen in Table 3, with the effect of the Hartmann number, the full vortex formation was completed at $h = 3.45$ for M = 0, while this value decreased considerably to $h = 2.07$ for M = 10.

It is clear that the magnetic field applied in the x-direction did not cause a change in the pattern of the stagnation point in the cavity. Also, interestingly, the symmetrical nature of the streamlines at M = 0 was preserved at M = 10. However, it had a significant effect on the full vortex formation such that the corresponding bifurcations for $\mathrm{S} = -1, 0, 1$ with M = 0 arose at a lower cavity height when M = 10.

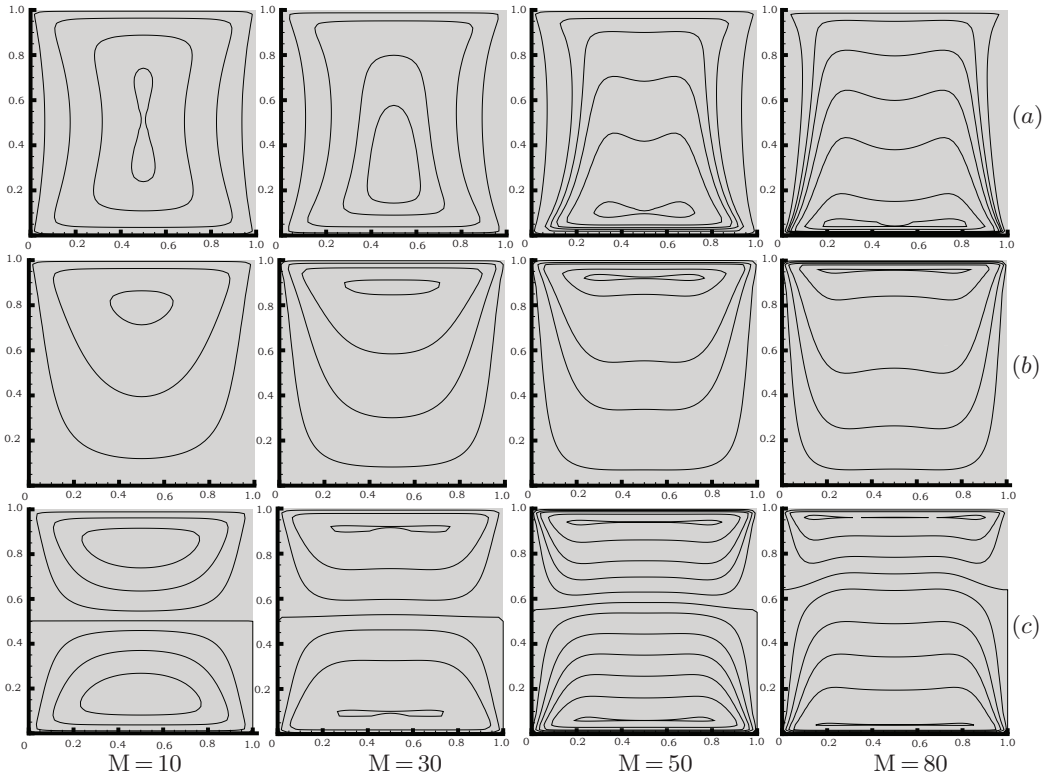

Fig. 6. Flow patterns in the region exposed to the y-directed magnetic field for (a) S = –1, (b) S = 0, (c) S = 1.

Table 3. Comparison of h values at which the flow pattern changes in the cavity at S = –1.

M = 0 (FDM)	M = 0 ([28])	M = 10
$h_{\mathrm{B.M}} = 2.98$	$h_{\mathrm{B.M}} = 2.934$	$h_{\mathrm{B.M}} = 1.87$
$h_{\mathrm{G.B}} = 3.26$	$h_{\mathrm{G.B}} = 3.225$	$h_{\mathrm{G.B}} = 1.99$
$h_{\mathrm{C.B}} = 3.45$	$h_{\mathrm{C.B}} = 3.400$	$h_{\mathrm{C.B}} = 2.07$

3.2. Results on the magnetic field acting in the y-direction. In this subsection, the changes in the streamline topology under the y-directed magnetic field are examined for different Hartmann numbers. First, let us examine the streamlines at different Hartmann numbers for $h = 1$. The solution of Eq. (12) is plotted for $\mathrm{S} = -1, 0.1$ with $\mathrm{M} = 10, 30, 50, 80$, and the flow patterns are shown in Fig. 6. One effect of the Hartmann number at $\mathrm{S} = -1$ is to disrupt the symmetry of the flow pattern for $\mathrm{M} = 0$. Indeed, at $\mathrm{M} = 10$, the center point above the saddle at (0.5, 0.5) gets closer to the saddle point with increasing Hartmann number, resulting in a cusp bifurcation, and turns into a full vortex. Because of the further increase of the Hartmann number, the velocity of the flow slows down considerably (see the center-line velocity profile in Fig. 7a). Accordingly, the center point lying on $x = 0$ gets closer to the bottom lid and turns into a saddle point, which is the pitchfork bifurcation.

In the case of $\mathrm{S} = 0$, the corner vortices have become too small to be affected by the magnetic field. As M increased, the center point on $x = 0$ bifurcated into the center and

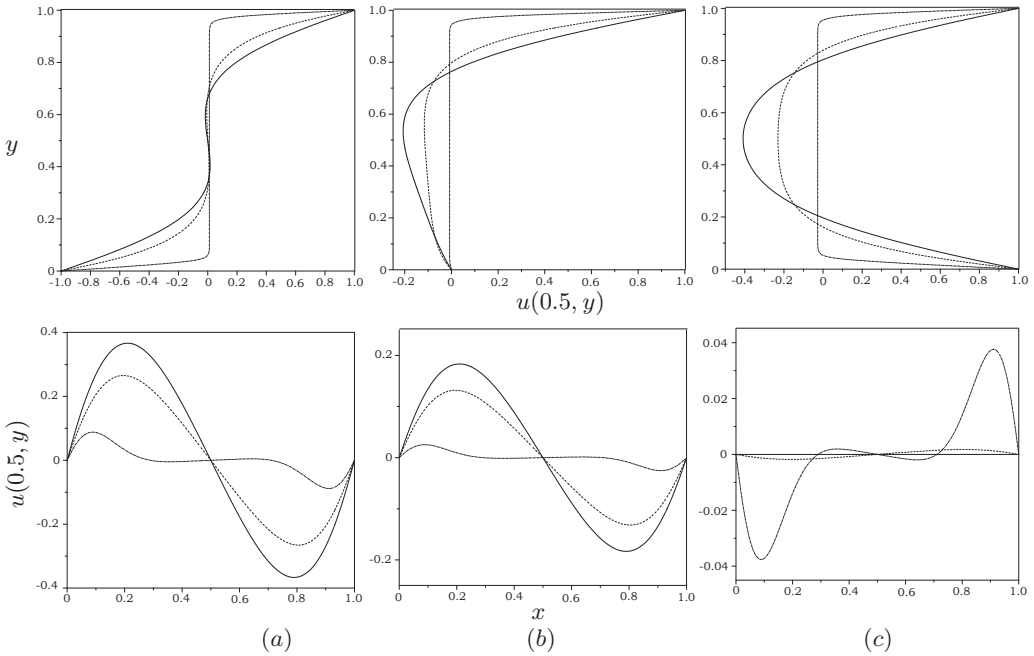

Fig. 7. Flow patterns in the region exposed to the y-directed magnetic field for (a) S = –1, (b) S = 0, (c) S = 1.

thus new stagnation points were produced, as with $S = -1$. While there was a velocity of the flow in front of the lid because of the movement, the flow became stagnant in the rest of the enclosure under the effect of the magnetic field and this caused the streamline to accumulate in front of the lid, see the graph of u at (0.5, y).

When the flow patterns were examined with the $v(x, 0.5)$ velocity profile for $S = 1$, it was observed that the separation line at $y = 0.5$ moved upwards under the effect of the Hartmann number and broke the symmetry of the cavity. Two center points located symmetrically along $x = 0.5$ turned into a saddle with two centers, one on each side, as M gradually increased. The upward movement of the separation line caused the flow to be trapped between the lid and itself. Hence, the same bifurcation arises in the central zone and produces a separatrix enclosing three sub-eddies.

Streamlines for $M = 10$ and $h = 5$ are plotted in Fig. 8. There is no difference in the flow patterns determined by $M = 0$. Indeed, with the increase of the cavity size, the corner eddies do not grow at $S = 0$ and the separation bubbles do not appear at $S = -1$ and $S = 1$. Therefore, the bifurcation sequences for $M = 0$ did not occur, and we observed no new vortex formation.

4. Conclusion.

In this study, the streamline behavior of the MHD Stokes flow in a rectangular region with the upper lid and the lower lid moving with $S = -1, 0, 1$ has been analyzed using a numerical method. The finite difference method was applied to obtain flow patterns throughout the region because it could solve such system of coupled equations without decoupling the equations and provided efficient results.

As the presence of the magnetic field in the x-direction did not cause a change in the bifurcation types in the cavity, a significant decrease was observed for the height values

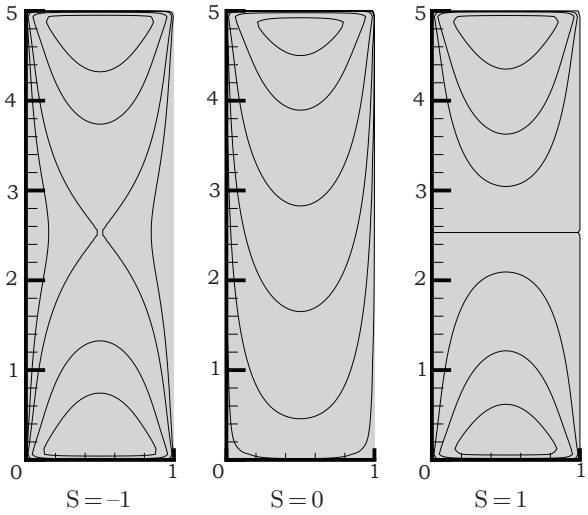

Fig. 8. Flow patterns for M = 10 and $h = 5$ under the magnetic field directed vertically.

at which the eddies completed their evolution. The Hartmann number had a different effect on the flow characteristics when the flow direction and the direction of the magnetic field were perpendicular to each other. By examining the center-line velocity profiles, especially u, it has been found that the flow slows down under the effect of the Hartmann number and tends to flatten, so it accumulates in front of the sliding lid. It is surprising that when the magnetic field acted in the y-direction, the streamline topology remained the same regardless of the length of the region (up to $h = 5$).

Acknowledgements.
This study was supported by Erciyes University Scientific Research Projects Unit, grant no. FKB-2020-10469.

References

[1] M. Tezer-Sezgin. Boundary element method solution of mhd flow in a rectangular duct. *International Journal for Numerical Methods in Fluids*, vol. 18 (1994), no. 10, pp. 937–952.

[2] A. Carabineanu, A. Dinu, and I. Oprea. The application of the boundary element method to the magnetohydrodynamic duct flow. *ZAMP Zeitschrift für angewandte Mathematik und Physik*, vol. 46 (1995), no. 6, pp. 971–981.

[3] H.W. Liu and S.P. Zhu. The dual reciprocity boundary element method for magnetohydrodynamic channel flows. *ANZIAM Journal*, vol. 44 (2002), no. 2, pp. 305–322.

[4] M. Tezer-Sezgin and C. Bozkaya. Boundary element method solution of magnetohydrodynamic flow in a rectangular duct with conducting walls parallel to applied magnetic field. *Computational Mechanics*, vol. 41 (2008), no. 6, pp. 769–775.

[5] B. Singh and J. Lal. Finite element method in magnetohydrodynamic channel flow problems. *International Journal for Numerical Methods in Engineering*, vol. 18 (1982), no. 7, pp. 1104–1111.

[6] B. Singh, J. Lal, and P. Agarwal. Finite element method for unsteady mhd channel flow with arbitrary wall conductivity and orientation of applied magnetic field. *Indian J. pure appl. Math.*, vol. 16 (1985), no. 11, pp. 1390–1398.

[7] Z. Demendy and T. Nagy. A new algorithm for solution of equations of MHD channel flows at moderate Hartmann numbers. *Acta Mechanica*, vol. 123 (1997), no. 1-4, pp. 135–149.

[8] K.E. Barrett. Duct flow with a transverse magnetic field at high Hartmann numbers. *International Journal for Numerical Methods in Engineering*, vol. 50 (2001), no. 8, pp. 1893–1906.

[9] M. Tezer-Sezgin and M. Gürbüz. Mhd convection flow in a constricted channel. *Analele Stiintifice ale Universitatii Ovidius Constanta, Seria Matematica*, vol. 26 (2018), no. 2, pp. 267–283.

[10] M. Gürbüz and M. Tezer-Sezgin. RBF solution of MHD Stokes flow and MHD flow in an constricted enclosure. *Turkish World Mathematical Society Journal of Applied and Engineering Mathematics*, vol. 11 (2021), no. 1, pp. 203–215.

[11] A. Sterl. Numerical simulation of liquid-metal mhd flows in rectangular ducts. *Journal of Fluid Mechanics*, vol. 216 (1990), pp. 161–191.

[12] P.-W. Hsieh, Y. Shih, and S.-Y. Yang. A tailored finite point method for solving steady MHD duct flow problems with boundary layers. *Communications in Computational Physics*, vol. 10 (2011), no. 1, pp. 161–182.

[13] M. Chutia and P. Deka. Numerical solution for coupled MHD flow equations in a square duct in the presence of strong inclined magnetic field. *International Journal of Advanced Research in Physical Science (IJARPS)*, vol. 2 (2015), no. 9, pp. 20–29.

[14] S. Arslan and M. Tezer-Sezgin. Exact and FDM solutions of 1D MHD flow between parallel electrically conducting and slipping plates. *Advances in Computational Mathematics*, vol. 45 (2019), no. 4, pp. 1923–1938.

[15] M. Gürbüz and M. Tezer-Sezgin. MHD Stokes flow in lid-driven cavity and backward-facing step channel. *European Journal of Computational Mechanics*, vol. 24 (2015), no. 6, pp. 279–301.

[16] N.F. Okechi, S. Asghar, and D. Charreh. Magnetohydrodynamic flow through a wavy curved channel. *AIP Advances*, vol. 10 (2020), no. 3.

[17] N.F. Okechi and S. Asghar. MHD Stokes flow in a corrugated curved channel. *Chinese Journal of Physics*, vol. 71 (2021), no. November 2020, pp. 38–53.

[18] P.N. Shankar. The eddy structure in stokes flow in a cavity. *Journal of Fluid Mechanics*, vol. 250 (1993), pp. 371–383.

[19] M.A. Kelmanson and B. Lonsdale. Eddy genesis in the double-lid-driven cavity. *Quarterly Journal of Mechanics and Applied Mathematics*, vol. 49 (1996), no. 4, pp. 633–655.

[20] F. Gürcan, P.H. Gaskell, M.D. Savage, and M.C. Wilson. Eddy genesis and transformation of Stokes flow in a double-lid driven cavity. *Proceedings of the Institution of Mechanical Engineers, Part C: Journal of Mechanical Engineering Science*, vol. 217 (2003), no. 3, pp. 353–363.

[21] F. Gürcan. Effect of the Reynolds number on streamline bifurcations in a double-lid-driven cavity with free surfaces. *Computers and Fluids*, vol. 32 (2003), no. 9, pp. 1283–1298.

[22] P.H. Gaskell, M.D. Savage, and M. Wilson. Stokes flow in a half-filled annulus between rotating coaxial cylinders. *Journal of Fluid Mechanics*, vol. 337 (1997), no. April, pp. 263–282.

[23] F. Gürcan and H. Bilgil. Bifurcations and eddy genesis of Stokes flow within a sectorial cavity. *European Journal of Mechanics, B/Fluids*, vol. 39 (2013), pp. 42–51.

[24] A. Deliceoğlu and E. Çelik. A mechanism of eddy generation in a single lid-driven T-shaped cavity. *Cumhuriyet Science Journal*, vol. 40 (2019), no. 3, pp. 583–594.

[25] A. Deliceoğlu, D. Bozkurt, and E. Çelik. Flow topology in an L-shaped cavity with lids moving in the same directions. *Mathematical Methods in the Applied Sciences*, vol. 43 (2020), no. 15, pp. 8317–8326.

[26] C. Pozrikidis. *Fluid Dynamics: Theory, Computation, and Numerical Simulation* (Springer Publishing Company, Incorporated, 2016), 3rd ed.

[27] F. Gürcan. Flow bifurcations in rectangular, lid-driven, cavity flows. Ph.D. thesis, University of Leeds, 1997.

[28] F. Gürcan and A. Deliceoğlu. Streamline topologies near nonsimple degenerate points in two-dimensional flows with double symmetry away from boundaries and an application. *Physics of Fluids*, vol. 17 (2005), no. 9, pp. 1–7.

Received 30.07.2021